

Integration, Test, and On-Orbit Operation of a Ka-band Parabolic Deployable Antenna (KaPDA) for CubeSats

Jonathan Sauder¹, Nacer Chahat², Brian Hirsch³, Richard Hodges⁴, and Eva Peral⁵
Jet Propulsion Laboratory, California Institute of Technology, Pasadena, CA, 91109

Yahya Rahmat-Samii⁶
University of California Los Angeles, Los Angeles, CA, 90095

Mark W. Thomson⁷
Tendeg, Louisville, CO 80027

In the past decade, CubeSats have undergone a revolution, moving from university research projects to enabling industry opportunities and government missions. Six years ago, the Jet Propulsion Laboratory, California Institute of Technology (JPL/Caltech) initiated a research and technology development effort to advance CubeSat communication capabilities, with one of the key thrusts being the Ka-band parabolic deployable antenna (KaPDA). This antenna started with the ambitious goal of fitting a 42 dB, 0.5 meter, 35 GHz antenna in a 1.5U canister. At that time, there had been very limited development in the area of high gain CubeSat antennas which are critical for both high data rate communications and remote sensing science. A Ka-band high gain antenna would provide a 10,000 times increase in data communication rates over an X-band patch antenna and a 100 times increase over state-of-the-art S-band parabolic antennas. This paper discusses the process of building, integrating, and operating the flight antenna, its final performance and lessons learned. KaPDA was an enabling technology for RainCube mission, the first Earth Science CubeSat to have an active instrument. RainCube was launched in May of 2018, making KaPDA the second deployable parabolic antenna to fly on a CubeSat and the first of its kind to operate at Ka-band enabling a number of opportunities for high rate, deep space antenna communications and remote sensing science.

I. Introduction

Cubesats have evolved tremendously in the last decade, going from university technology development research projects, to becoming science enabling and creating new business opportunities. While originally most missions were restricted to Low Earth Orbit (LEO), CubeSats have begun to increase their reach across the solar system with the advent of Mars Cube One (MarCO) in 2018 [1]. As operational distances between CubeSats and Earth increase and instruments become more advanced, data rates are a mission-limiting factor. Improving CubeSat data rates became critical enough for NASA to establish the CubeQuest Centennial Challenge [2] where one of the key metrics is transmitting as much data as possible from the moon and beyond. Currently, many CubeSats communicate on UHF bands, with those that are viewed as having high data rate abilities using S-band or X-band patch antennas. The CubeSat ANEAS,

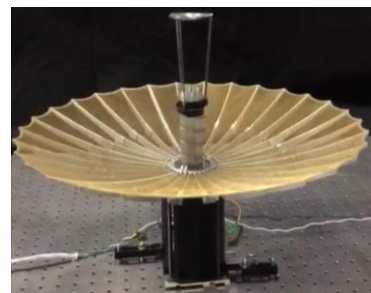


Figure 1. KaPDA

¹ Mechatronics Engineer, Technology Infusion, 299-101, 4800 Oak Grove Drive, Pasadena, CA, AIAA Member

² RF Engineer, Spacecraft Antennas, 161-260, 4800 Oak Grove Drive, Pasadena, CA

³ Mechatronics Engineer, Deployable Structures, 299-101, 4800 Oak Grove Drive, Pasadena, CA, AIAA Member

⁴ Senior Principal Engineer, Spacecraft Antennas, 161-260, 4800 Oak Grove Drive, Pasadena, CA

⁵ SWOT KaRIn Lead System Engineer, 161-260, 4800 Oak Grove Drive, Pasadena, CA

⁶ Professor, Electrical Engineering, 6731K Boelter, 420 Westwood Plaza, Los Angeles, CA

⁷ Chief Technology Officer, 1772 Prairie Way, Unit A, Louisville, CO, AIAA Associate Fellow

which was launched in September 2012, pushed the envelope with a half-meter S-band dish which could achieve 100x the data rate of patch antennas. A half-meter parabolic antenna operating at Ka-band would increase data rates by over 100x that of the ANEAS antenna and 10,000x that of X-band patch antennas. Further, various radar missions are enabled by large aperture high frequency parabolic antennas. This would be particularly useful for Earth-monitoring CubeSat constellations.

II. Background

Several deployable parabolic and parabolic-like antennas have been investigated in the past for CubeSats. Concepts prior to KaPDA have included a goer-wrap composite reflector [3], a reflector transformed from the CubeSat body[4], an inflatable parabolic reflector with reflecting material on one side and transparent material on the other[5], a mesh reflector supported by ribs [6,7], and a folded panel reflectarray [1,8–10]. While these designs provide unique solutions, they were all designed to operate at S-band (with the exception of the reflectarray, which is also currently under development at the Jet Propulsion Laboratory). A Ka-band antenna has much greater gain, which translates to greater data rate, but requires a much higher surface accuracy than an S-band antenna. The lack of high gain antennas motivated JPL to launch a research and development effort for high frequency deployable antennas for CubeSats three years ago.

Deployable antenna concepts can be organized by architecture, each of which have strengths and weaknesses in meeting CubeSat communication needs. Architectures include solid deploying reflectors, shape memory reflectors, inflatables, folded panel reflectarrays, inflatable/thin-membrane membrane reflectarrays [11] and mesh reflectors. Solid deploying reflectors have great surface accuracy, but do not stow well in small spaces and can be heavy (e.g. Hughes spring-back antenna [12]). Shape memory reflectors may work at lower frequencies, but much development is still required as, at Ka-band, the surface is not accurate enough [13]. Inflatable reflectors stow well and are lightweight but have issues with maintaining inflation and shape. This is especially problematic on interplanetary CubeSat missions which will likely last much longer than LEO CubeSat missions. Reflectarray antennas provide a relatively high gain and stow well in large flat spaces (i.e. areas for solar panels on a CubeSat), but reflectarrays have inherent bandwidth limitations and the antenna gain is constrained by the number of panels that can practically be stowed and deployed. Therefore, the mesh reflector architecture is a very attractive deployable high gain antenna design for many applications.

There are many concepts for mesh parabolic deployable antennas at much larger scales than CubeSats. In the 1970's Lockheed Martin developed the Wrap-Rib reflector, which uses a mechanism to wrap the ribs and mesh like a tape measure [14]. However, the design does not fit well in the CubeSat form factor as the mechanism that deploys and stows the ribs is quite large. There are also a number of knit mesh reflectors, the most popular of which are Harris's Unfurlable Antenna [15] and Northrop Grumman's AstroMesh [13]. However, these two designs consist of many small, detailed components, which are challenging to scale down without the antenna becoming prohibitively expensive. It should be noted that about two years after the start of JPL's initiative, others began developing CubeSat antenna designs inspired by the AstroMesh and Unfurlable Antenna configurations, but both have larger apertures and are likely to consume more volume than the antenna discussed in this paper [9,16].

At the point the Ka-band antenna effort began three years ago, two knit mesh antennas had been developed for CubeSats, but both were designed for S-band operation. They were a spiral stowed rib design [7] and the Aneas parabolic deployable antenna (APDA) folding rib design that was used on USC/ISI's Aneas spacecraft [6]. The spiral stowed rib design, while very compact, would be challenging to extend to Ka-band as the ribs could not apply adequate force required to stretch Ka-band mesh to achieve the required surface accuracy. The APDA architecture would work well for Ka-band as it used straight folding ribs thereby applying more force and allowing for greater surface accuracy. In addition, the APDA is the only CubeSat parabolic deployable antenna to have flown. Therefore, it was decided to use the APDA as a starting point for the Ka-band parabolic deployable antenna (KaPDA) design [17,18].

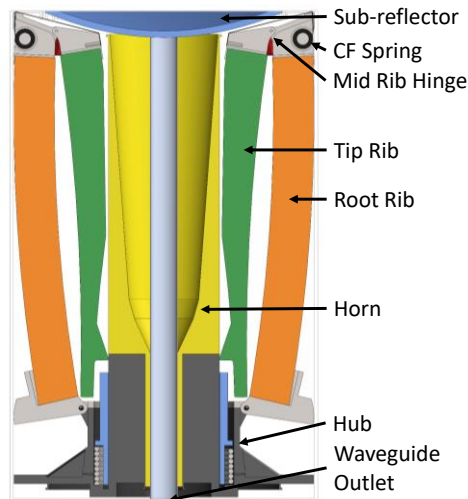


Figure 2. Key KaPDA Components

III. KaPDA Design Overview

The first design task was to analyze the influence of antenna configurations on stowed space and gain. A number of designs were explored including Cassegrainian, Gregorian, and several hat-style feeds [19,20]. The Cassegrainian configuration was selected as it best balanced performance and stowed size (the dimensions for the subreflector were such that it could be stowed within 1.5U).

The number of ribs supporting the mesh structure was a key factor for achieving surface accuracy which is critical at Ka-Band. More ribs result in a more ideal dish and thus, greater radio frequency (RF) gain. However, as the number of ribs increase, the clearance between each rib when stowed decreases. Packing ribs too tightly could result in snagging during deployment. The best compromise between rib clearance and RF loss was found to be 30 ribs.

Each rib was divided into two components, the root rib and tip rib, which were connected by the mid rib hinge. The mesh forces and resulting moments determined the geometry of the rib. As the root ribs experienced the greatest bending moment, they were deeper. The tip rib had a tapered design to conserve space and eliminate material where it was not required for rigidity. The taper was designed to create an even stress profile throughout the rib. To improve both stowing efficiency and surface accuracy, the ribs were much deeper (by over 10 times) but slightly thinner than those used on APDA. The deep rib design was also advantageous for precisely controlling the ribs' deployed position.

Perhaps the greatest design challenge was developing a deployment mechanism that stowed in 1.5U with the antenna. The deployment mechanism must first push the hub out of the CubeSat and then unfold the ribs. The APDA was deployed entirely using springs, with all the components unfolding quickly. However, Ka-band requires 40 opening per inch (OPI) mesh which is stiffer and required greater deployment forces than the 10 OPI mesh APDA used. A preload of approximately 250N was required at the end of the spring's displacement, which means any stowed spring would likely be compressed to well over 500 N resulting in a violent deployment. Therefore, it was necessary to explore concepts other than springs for deploying the hub and ribs.

To deploy the hub, a number of concepts were explored including a motor driving a threaded rod, a scissors lift, low force springs (if hub deployment was decoupled from rib deployment), cables and pulleys driven by motors, and a gas driven piston. Many concepts were eliminated because of complexity (e.g. cables and pulleys driven by motors), they were challenging to implement within the highly constrained space (e.g. scissors lift), or they didn't work (e.g. low force springs). An approach using lead screws to actuate the antenna upwards was ultimately selected. Four lead screws were located in the four corners of the cylinder, driven by a 12 mm Faulhaber motor and a 256:1 gearbox. The lead screws were aligned to keep the hub plate flat through shimming, which also kept the antenna aligned with the waveguide during deployment. The lead screws were constructed of 10-32 threaded rods, which were threaded into a 64 tooth gear. To keep the lead screws in sync with each other, the "planet" gears were attached the base of each lead screw meshed with a "sun gear". One of the lead screw gears was driven by a motor, and the motor's torque was then transferred to the other three lead screws via the sun gear.

To deploy, the lead screws first drove the hub upwards (Figure 3, A-B). As the hub reached the top of the canister, the root rib hinges caught on the edge of the canister and the ribs began to deploy (B-C). When the tip ribs reached the point where they become free of the horn interference, a constant force springs deployed them (Image C). The hub continued to travel upwards until the root ribs fully deployed (image D). The hub also contacted several limit switches, to confirm deployment. As the root ribs fully deployed, the root rib hinges released the subreflector and it telescoped along the horn, pushed upward and held in place by a spring (C to D). The lead screws maintained a preload on the antenna in the deployed position.

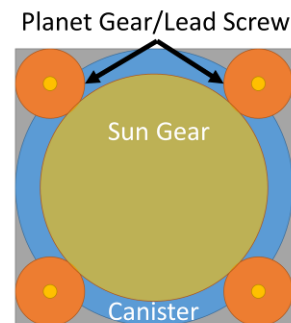


Figure 3. Four Lead Screws Provide a Level, Controlled Deployment

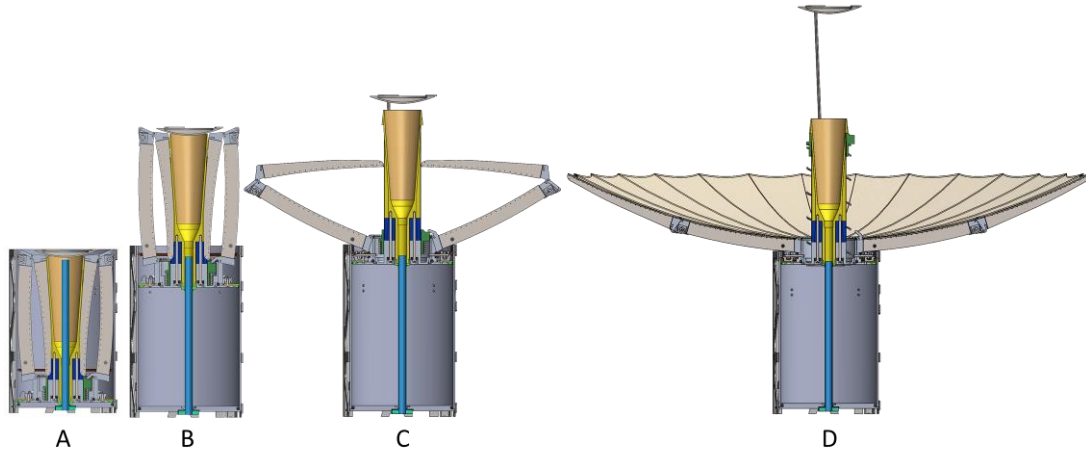


Figure 4. KaPDA Deployment Sequence

The motorized design provided a number of other advantages beyond a controlled deployment and keeping the hub axially aligned with the waveguide. It also eliminated the need for all latches and a launchlock, as preload from the lead screws was used to secure the antenna in the stowed position and retain it in the fully deployed position. Given the low pitch of the lead screws, it was virtually impossible for launch or deployment loads to back drive the screws, thus providing a secure latch. Using a motorized deployment provided a controllable deployment sequence as a motor controller governed motor rate and position of the antenna and the encoder provided feedback on the number of shaft revolutions providing deployment status.

IV. Qualification Testing of the Engineering Model Antenna

For performance qualification, an engineering model of the antenna was constructed. Prior to deploying the antenna, it was tested in the as-built state on a planar RF range at JPL. The test resulted in a gain of 42.5 dBi. After deployment a second RF test resulted in a performance of 42.6 dBi. In general RF tests are accurate to within +/- 0.2 dB, therefore the slight variance in the results was expected.

After the motorized deployment mechanism was successful demonstrated, the upgraded engineering model antenna was stowed and subjected to a series of vibration tests simulating launch loads. The goal was to qualify the antenna to the General Environmental Verification Standard (GEVS) protoflight levels [21], at 14.1 G_{RMS} in three axes. To determine the antenna response, accelerometers were mounted on both the antenna canister and the subreflector. Random vibration tests began at low levels and progressed through multiple tests until qualification levels were reached. A low-level vibrational sine sweep and hardware inspection occurred after each random vibration test. If there was a significant shift in the sine sweep, this could indicate a structure change, and thus damage. After the 7 G_{RMS} test in the Y-axis, significant changes in the sine sweep were observed. Several dynamics experts were consulted for advice, and it was determined because the antenna contained a number of “loose” ribs, as the mid-rib hinges were free to rotate slightly, the variations in sine sweep response were not a good indicator of a loss of structural integrity. A simple shift in the position of the hinged components could lead a different response. The dynamicists suggested a better indicator than the sine sweep would be to instead perform a low-level random vibration test, at 1.77 G_{RMS} before and after each test. Because the stochastic nature of the random vibration test, it should average the differences in hinge position at a specific frequency, and thus be a better indicator of structural integrity.

Table 1 Comparison of KaPDA Performance.

Measure	Units	Goal	Prelim. Design	Pre-Deploy	Post Deploy	Post Vibe
Stowed Size	U (10x10x11.3cm ³)	1.5	1.36	1.43	1.43	1.43
Deployed Diameter	m	0.5	0.51	0.51	0.51	0.51
Gain	dB	42	42.6	42.5	42.6	42.7
Mass	Kg	3.0	1.9	1.2	1.2	1.2
Thermal	°C	-17 to 35	--	0 to 55	0 to 55	0 to 55

While this approach initially produced more consistent results, when switching the antenna from the Y-axis to the X-axis, and performing a 10 G_{RMS} vibration test, the results from the pre and post 1.77 G_{RMS} response seemed to indicate a structural shift. To ensure there was no damage before proceeding with the more intense 14.1 G_{RMS} test, it

was deemed necessary to deploy the antenna.

After deployment, the antenna appeared to be in the same condition as it was prior to vibration, with no indications of damage. The question remained, if the structure was not completely fixed inside the antenna canister, could this lead to variations in the random vibration response, and was it not averaged as was originally expected? To answer this question, additional sources of data were examined. A similar situation to loose ribs in a canister occurs with a CubeSat inside a generic P-POD deployer; where the CubeSat is free to move. In comparing low-level random vibration tests of a CubeSat in a P-POD to the antenna, similar trends were observed. In some axes, the low-level random vibration tests aligned, but in others they did not. Therefore, it was determined for structures that are not fixed, it is normal for both the pre and post sine sweeps and the random vibration tests to not align, although the pre and post low-level random tests are more likely to align.

The test campaign continued with a 14.1 G_{RMS} vibration test in all three axes, which proceeded without incident. The engineering model antenna was successfully deployed after the vibration test and was taken to the RF range to analyze performance. No changes were found in performance before or after the vibration test with a measured gain of 42.7 dBi. Nearly as impressive as the post vibration performance was the fact the antenna was deployed over a half-dozen times, and consistently held the same performance.

V. Integration and Testing the Flight RainCube Antenna

Successful demonstration of KaPDA after vibration meant construction could begin on the flight Ka-band Radar Parabolic Deployable Antenna (KaRPDA) for RainCube [22], a precipitation Ka-band radar mission. RainCube is a technology demonstration mission validating the first active instrument in a CubeSat. This means that instead of observing signals from other sources, RainCube creates and then measures the reflection of its own signal. Several improvements were made between the engineering model and the flight model, including a geometry adjustment to the mid-rib hinges to increase torque margin, addition of features to better constrain the ribs during vibration, and minor changes to the sub-reflector and canister to provide more clearance during deployment [23]. Construction of the flight antenna began in the spring of 2016 and was completed in October 2016. The following outline summarizes steps during integration and test of the flight antenna.

1. RF pattern was measured prior to first stow and deployment.
2. Antenna was deployed at hot temperature, 65°C, in thermal vacuum.
3. RF pattern was measured after thermal vacuum deployment.
4. Antenna was integrated into radar instrument assembly.
5. Integrated instrument assembly underwent a 6.2 G_{RMS} workmanship vibration test.
6. The integrated instrument assembly was placed in a thermal vacuum, with the antenna deploying at cold, at 0°C.
7. The integrated instrument assembly was then be integrated with the spacecraft bus at Tyvak.
8. Antenna deployed in the lab during the instrument functional check after spacecraft bus integration.
9. Integrated spacecraft vibration test occurred at 2 G_{RMS} .
10. Integrated spacecraft was tested in thermal vacuum with antenna first motions.
11. Full final deployment of the antenna after thermal vacuum in an EMI shielded tent.

To visualize the components listed above, Figure 5 illustrates the three nesting assemblies which consisted of the antenna (KaRPDA), the integrated instrument, and the integrated spacecraft.

A. Testing Prior to Instrument Integration (Step 1)

There are three types of antenna deployments, a full deployment where the antenna was deployed 140mm to fully open, a first motion, where the antenna was driven forward by about 75mm, and then reversed, and a second motion, occurring after the antenna was deployed, where the antenna was stowed by 3.2 mm to verify positive torque margin without folding the deployed ribs.

The first test prior to integrating the flight antenna with the instrument was a thermal vacuum test, given the engineering model antenna had never been tested in the space environment.

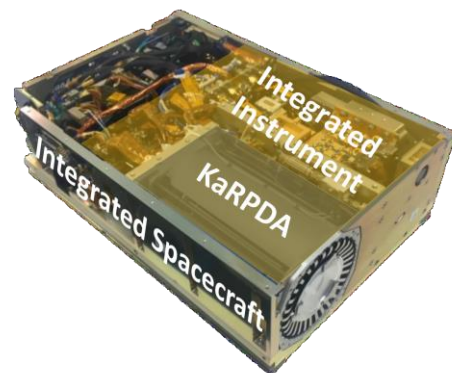


Figure 5. Assemblies nest within each other

This was more relevant than a vibrational test, as RainCube was going to be launch by NanoRacks, which meant the satellite would be provided with a soft-stow 2 G_{RMS} vibrational environment in a cargo launch to the International Space Station (ISS). As the engineering model had been previously tested to 14.1 G_{RMS} and survived, it was decided vibration testing of the flight model could wait until a higher level of assembly.

There was some debate if the antenna should first be deployed at the cold temperature (which would be the most difficult situation for the mechanisms) or at the hot temperature (which would be the most difficult situation for the motor drive electronics). Ultimately, it was determined that the hot deployment should occur first, as there was a strong desire to have the cold deployment after vibrational testing of the system, which didn't occur until steps 5 and 6. A cold deployment immediately succeeding the vibrational test has the least deployment force margin as vibration ensured the spring deployment mechanisms were at their lowest state of potential energy, and the cold temperature meant the grease was thicker, further resisting deployment. To deploy at cold after vibe, demonstrated the mechanism had positive margin for the worst-case scenario.

Originally, the plan for the hot thermal vacuum deployment was to deploy the antenna at 65°C, which provided 20°C margin over the maximum on orbit expected deployment temperature of 45°C. The chamber was first heated to a protoflight hot non-operational temperature of 75°C, and then cooled to 65°C. After asymptoting at 65°C, deployment commenced but the motor controller paused halfway through the deployment and stopped issuing commands to the motor. After performing several additional tests, it was determined the motor controller quickly overheated to 85°C in the hot, vacuum condition (in less than 2 minutes). This was due to not having an adequate thermal path in vacuum for the microchip on the commercial-off-the-shelf (COTS) controller, which was designed to have air to cool the chip. To remedy the situation, the chamber temperature was reduced by 10°C to 55°C. The antenna was then operated in a series of first motions for 8 minutes, or 2.5 time longer than the deployment time of about 3 minutes. It was observed the motor controller temperature asymptoted to 78°C, below the 85°C motor controller temperature limit. This indicated it was safe to proceed with a deployment at 55°C, which occurred successfully a few minutes later. The chamber was then taken to a protoflight cold non-operational temperature of -35°C, and after dwelling for 2 hours, was heated to 0°C, where a second motion occurred to verify the antenna drive mechanism worked at cold. The results of this test levied new requirements on spacecraft operations, specifically that the antenna would need to be between 10°C and 40°C during deployment, when including margin. The 40°C number was reached by reducing the test margin from 20°C to 15°C for the demonstrated deployment at 55°C. Another option would have been to redesign the aluminum chassis, which contained the COTS controller, to provide better thermal path for the microchip, but thermal models indicated there would be many times when the spacecraft was below 40°C during nominal operations. The 10°C limit at the low end was reached by having 10°C of margin (which should be noted is 5°C less than the preferred 15°C of margin) over the 0°C cold test condition. The 0°C cold test was set by the glass transition temperature of the solithane which lines the edges of the mesh, which has a glass transition temperature of around -10°C. If the solithane was brittle, it would have been subject to cracking during the motion of deployment.

After deployment in thermal vacuum, the antenna was then tested for RF performance, and found to have a similar gain to the engineering model antenna. This was the last RF test for the antenna, as it could not be tested after being integrated with the instrument.

B. Integration into Instrument and Testing (Steps 2-4)

After the thermal vacuum test, the antenna was integrated into the spacecraft instrument. A total of eight 6-32 socket head cap screws were used to attached the antenna to a half-inch thick aluminum structure called the "T-plate" which was also used to hold the rest of the instrument. This T-plate was also the primary structure which was used to attach the instrument to the spacecraft bus, and provided a single interface for handling fixtures.

Having the instrument and antenna mounted to one structure also made it easy to vibrate the entire assembly. While the instrument saw very low level of vibration during launch, a 6.2 G_{RMS} workmanship vibration test was performed. This ensured all structural interfaces were bolted as expected. Post vibration, the integrated instrument was placed in thermal vacuum. The chamber temperature was first raised to 65°C to evaporate any moisture in the assembly and then was cooled to the cold non-operational temperature of -35°C. After dwelling for several hours, the temperature was raised to 0°C, where the antenna was deployed. This time, the antenna deployed exactly as expected. The instrument was then thermally cycled between 75°C and -35°C with second motions occurring at 55°C and 0°C to ensure expected operation.

The successful completion of thermal vacuum meant the integrated instrument had been fully qualified, and attention was turned towards integrating the instrument to the spacecraft. In reviewing the integration procedure, it was discovered that while the deployments in thermal vacuum had occurred at 5.5V, the spacecraft would be supplying between 9V to 12V to the antenna. This led to an investigation with the engineering model unit to

understand how voltage influenced the antenna performance. It was observed as voltage increased, power consumption also increased slightly. It was also found that when the motor stalled, a higher stall torque was achieved. This put several of the components in the antenna system at risk of yielding. To protect against this, the motor controller was programmed to limit the maximum current draw from 2.8A to 1.5A.

C. Integration into Spacecraft and Testing (Steps 5-9)

The integrated instrument was then transported to Tyvak, and installed on the spacecraft bus. After performing a number of checkouts, the antenna was then given the command to deploy. The antenna began to deploy, but then stopped after traveling about 75mm, or just before the ribs began to pivot. Investigation revealed that a position limit had been set on the motor controller in earlier in testing, and the position limit had not been removed. When the controller was powered on, the position limit was persistent. The position limit was manually deactivated, and the antenna was reversed to the stowed state, and then commanded to deploy again. This also created a change in the approach to the flight deployment script, where the position limit would be deactivated before deploying.

This time the antenna fully deployed, however after deploying the motor kept driving until it almost stalled. Up to this point, the position had been slowly increased for each deployment, to achieve the maximum amount of preload (calculated by multiplying the number of steps in the motor, by the gear ratio in the motor gearbox, by the gear ration between the motor pinion and planet gear, and finally the pitch of the lead screws). The last commanded distance in the prior deployment was 137.7mm, and it had been increased to 140.5 mm in deployment distance. While this was initially calculated to have clearance, it turned out to be a bit too far, as it was noticed from the motor behavior that it nearly stalled (which was undesirable due to the forces a stall generates). It was realized the exact calculations of distance did not quite line up with the actual distance traveled, likely due to backlash in the gear system. It was noted for future deployments, that the distance should be 140.3 mm to achieve full preload, without allowing the motor to stall. In reviewing the motor data, it was also noted that the spacecraft did not capture current and voltage during deployment, as the final version of the flight software had not yet been released. As such, only data from the motor controller related to position, temperature, and time were collected.

The antenna was then stowed, and the integrated spacecraft was then transported to a vendor facility for vibrational testing at 2 G_{RMS} . After vibrate, the integrated spacecraft was then transported back to Tyvak for thermal vacuum testing. As the integrated spacecraft was a larger assembly, and as the thermal vacuum chamber at Tyvak was smaller, it was impossible to deploy the antenna during thermal vacuum testing. Instead, first motions were used to drive the antenna backwards and forwards for the first 75mm until it was driven for three minutes. The first motions were performed at both hot 55°C and cold 0°C. To prevent the antenna from deploying in the small chamber, which would have had disastrous consequences, the position limits were also activated during this test. Once again, only controller telemetry was captured due to not having the final flight software. After completing thermal vacuum, the integrated spacecraft was transported to an electro-magnetic interference (EMI) shielded tent, to simulate an RF environment similar to space. The position limits were turned off, and the antenna was then deployed via a simulated ground station, which provided a dry run of the antenna deployment. The final version of the flight software was used during this final deployment, so both motor controller data, as well as voltage and current data were captured.

After deploying, a final stow operation was performed. After about 6 mm the antenna stopped moving, and would not drive any further. The system was then power cycled, and the antenna began to stow again, but once again stopped after 6 mm. First, the communication lines and protocol between the spacecraft and simulated ground station were checked, to ensure there were not unexpected behaviors, but no obvious issues appeared. Through further investigation, it was realized the position limit was never turned off (only the script for deploying, and not the one for stowing, automatically deactivated the position limit), and the default state for the position limit after power cycling was “on”. As such, the antenna was cutting the stow distance short, due to the position limit. The position limit was then turned off, and the antenna was finally successfully stowed. After this experience the upper position limit was changed from 76546171 steps (82.6mm) to 131302400 steps (141.6mm) and the lower position limit from -5888000 steps (-6.4mm) to -131302400 steps (-141.6mm). With the new position limits set, the payload was ready for launch in March 2018, and inserted into the NanoRacks dispenser in Houston.

VI. On Orbit Performance

A. Deployment Operation on Orbit

RainCube was manifested on the ELaNa-23 flight with six other CubeSat Launch Initiative (CSLI) missions. On May 21st, 2018, RainCube was launched on Orbital-ATK’s OA-9 ISS resupply mission as part of the soft cargo. After launch, RainCube stayed on the ISS for almost two months awaiting an opportunity to be ejected from the

NanoRacks dispenser. On July 13th, 2018 at 1:05 AM PDT, RainCube was released to become a free flier. After several weeks of commissioning and ensuring the spacecraft was healthy, the first attempt to deploy the antenna occurred on July 27th.

Table 2. On Orbit Versus Lab Performance

	Ground Test 1	Ground Test 2	Orbit	Target
Time	02:54.0	02:53.7	02:53.7	--
Position	130320283	130067786	130086265	130084760
% Deviation	0.181%	-0.013%	0.001%	0.000%
Deviation in mm	0.254	-0.018	0.002	0

Antenna deployments where strategically scheduled to align with at least three ground passes in a row. During the first ground pass, the antenna was given a checkout script, which checked the configuration of the motor controller and all the parametric values, but stopped just short of commanding the antenna to move. The checkout results were downlinked on the second ground pass. The team had approximately 50-60 minutes to review the data, before making a call whether to upload the deployment commands on the third pass which occurred 90 minutes after the second pass. On the third pass, the full deployment commands were sent, telling the antenna to deploy at a time when its orbit was calculated to meet the following requirements:

- 1) The radar antenna could not be deployed or powered on while the RainCube vehicle was over the South Atlantic Anomaly, due to risk of radiation interrupting the critical operation.
- 2) The radar antenna could only be deployed while the RainCube vehicle was over areas of low radiation, within +/- 20 degrees of the equator.
- 3) The radar antenna could not be deployed if the radar control surfaces were predicted to be below +10C or above +40C throughout the 3 minute deployment operation.
- 4) They deployment *should* occur when the antenna was properly illuminated for the deployment to be captured on the spacecraft’s camera (this was a “desirement”)

After the first pass on July 27th, the telemetry from the motor controller was downlinked. All data appeared nominal, except for the motor controller position limits. While the position limits were deactivated, the upper position limit was 76546171 steps and the lower position limit was -5888000 steps. This caused some confusion, as the position limits were just changed before loading the CubeSat into the NanoRacks dispenser. It appeared the motor controller had changed the position limits on its own, which led to concern. This caused the team to scrub the deployment for the day. After reviewing the procedures from setting the position limits, it was realized the position limit changes were never saved after being set just before being loaded into the dispenser. As such, the position limit reverted to its old values when rebooting. As root cause was determined, deployment was scheduled to proceed on the next day. Further, as the position limit was deactivated at the start of the deploy script, it was determined to not attempt to change the position limits as uploading new scripts to change the position limits represented a greater risk than deploying with the limits as is, given they were deactivated.

On July 28th, the antenna was sent the command to deploy. About 10 minutes after deployment, a ground pass occurred. However, given the very limited data rates, only current data for the motor and telemetry from deployment limit switches on the antenna were downlinked. The motor appeared to have drawn the right amount of current for the right amount of time (give or take 10 seconds), and all the limit switches were triggered, indicating deployment was likely successful. Several hours later the next data set was downlinked, this time motor encoder telemetry. This confirmed that the motor had reached the right number of steps to fully deploy the antenna. Finally, on the morning of July 29th, a high data rate pass occurred, and images from the spacecraft on board camera were downlinked, and showed a fully deployed antenna. Radar performance data later confirmed that the antenna surface figure was perfect.



Figure 6. Antenna Deployment Sequence on Orbit

B. Analysis of On Orbit Results

One of the first metrics for comparison between ground tests and on orbit performance was the number of steps the motor made on Earth deployments, versus the number of steps on orbit. Deployment time was also compared.

The target number of steps for deployment was 130084760. In comparing the number of steps on orbit versus the two ground deployment tests, it was found that on orbit the antenna achieved a position that was closer to its desired target (Table 2). It should be noted that Ground Test 1 occurred when the antenna was deployed slightly too far, hence the slightly longer deployment time and slightly greater deviation from the target value.

The second piece of motor controller telemetry compared was the temperature of the motor controller microchip versus deployment time. The ground tests started with the motor controller at 30°C and 29°C, and the on-orbit test started with the chip at 31°C. However, during the deployment, the chip on orbit warmed by 5°C more than the ground tests, due to the lack of convection.

The next piece of telemetry compared was the power draw of the antenna on orbit, versus the power draw of the antenna during the ground tests. On orbit, the antenna was found to draw 8.1% less power. From a graphical perspective (Figure 7), this difference is almost negligible. Also, given only one ground data set was available in the flight configuration, it is hard to know how much variance there would have been in multiple ground test data sets. Even so, the lower power draw could be attributed to three effects. First, on orbit it appears the antenna was 2°C warmer than the ground deployments. This meant the grease was slightly thinner, and the mechanisms would have moved more freely. The second was gravity. On Earth, the antenna was deploying against gravity, meaning it would have to lift the weight of the antenna against gravity. This in turn meant the normal forces on the lead screws, and thus the total frictional forces were higher. Finally, the voltage on orbit was slightly lower at 12.0V instead of 12.2V during the ground test. Earlier testing had found that operating at a lower voltage would decrease power consumption.

The final element of performance was to compare a picture of the antenna deployed in the lab, to one of the antenna deployed on orbit (Figure 8). As the camera was in the same position, the images could be overlaid, which showed an exact alignment for the ribs and sub-reflector.

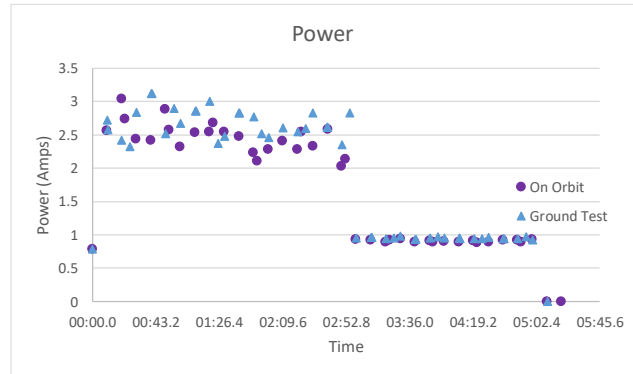


Figure 7. On Orbit versus Ground Power Consumption

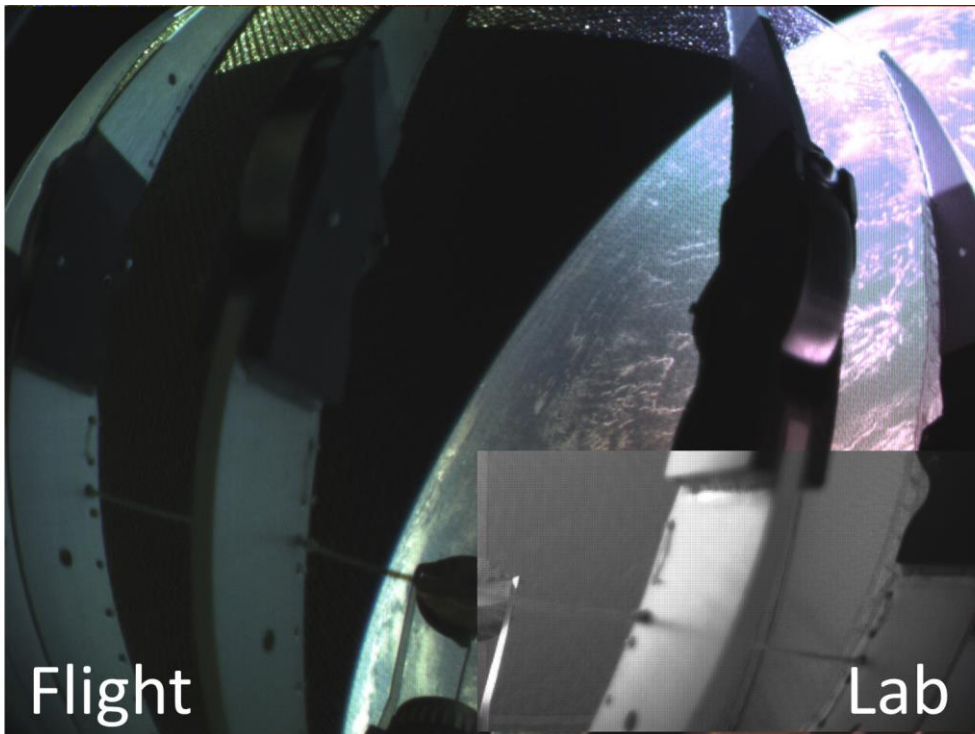


Figure 8. Comparison of a photo from the lab and on orbit confirmed a perfect deployment.

VII. Lessons Learned

There were a number of lessons learned, many of which were related to mechanism design, which have been previously captured [23,24]. However, as the integration and test campaign proceeded, there were a number of electrical and software lessons learned which are summarized here. When designing a deployment mechanism, especially for CubeSat programs which tend to be fast paced and have a single person wearing many hats, it just as important to take the time to fully understand the electrical and software aspects of the mission, as the mechanical system. Key lessons learned in this area were:

- 1) Consider thermal-electrical performance, especially in the absence of convection. This is especially true of COTS parts, which are often designed to cool from natural convection. Designing additional conductive thermal paths may be required, and would have allowed a higher deployment temperature for KaRPDA.
- 2) Ensure all requirements from the spacecraft bus are clear, and review them with the spacecraft team and mechanism team in person. Understand there are ranges of voltages which are easier for a spacecraft to provide, and know those voltages ahead of time. This would have reduced additional testing for KaRPDA.
- 3) Capture electrical behavior early. If something had gone wrong with KaRPDA, it would have been challenging to troubleshoot given there was only one ground test, the final deployment, with full telemetry. Capturing earlier tests using an oscilloscope when the final flight software was not yet written, would have been valuable.
- 4) When using a COTS component, with firmware/software installed, it is critical to understand how the firmware/software operates, and how the firmware operates in anomalous conditions (for example if suddenly powered off, what state does it boot-up in). Misunderstanding how the position limits operated on the motor controller added a lot of unneeded concern and failure investigations.

VIII. Conclusion

The Ka-band Radar Parabolic Deployable Antenna (KaRPDA) was successfully operated on orbit and still is an enabling technology for the RainCube mission. The antenna had a mass of 1.6 kg, stowed in a 97 x 97 x 161 mm volume, and deployed to 0.51 meters in diameter producing 42.6 dB of gain at 35.75 GHz. The antenna is still operating, providing valuable scientific data on weather patterns. The design has been licensed to Tendeg for commercialization, and they have received their first commercial order. The antenna has also been baselined in a number of new JPL Earth Science and interplanetary mission studies, indicating the far reaching impact of this technology.

Acknowledgments

The research was carried out at the Jet Propulsion Laboratory, California Institute of Technology, under a contract with the National Aeronautics and Space Administration. The authors thank Leah Ginsberg, David Hunter, Ted Steiner, and Savannah Velasco student interns, for their work on the mechanical design, Michael Johnson, Michelle Easter, Josh Ravich, and Kim Aaron who provided advice on the design, Brian Merrill (Spectrum Marine and Model Services), Hugo Rodriguez, Pedro Moreira, Natalie Lockwood-Barajas, Gerry Gaughen, Building 103 Techs and Rudy Herrera who assisted in building the antenna, and Dr. Jefferson Harrell who performed the RF tests.

The authors of this paper also wish to thank all of the RainCube spacecraft and instrument team members. The JPL team includes The JPL team includes Shannon Statham, Shivani Joshi, Simone Tanelli, Travis Imken, Douglas Price, Chaitali Parashare, Alessandra Babuscia, Elvis Merida, Marvin Cruz, Carlo Abesamis, Macon Vining, Joseph Zitkus, Richard Rebele, Mary Soria, Arlene Baiza, Stuart Gibson, Greg Cardell, Brad Ortloff, Brandon Wang, Taryn Bailey, Dominic Chi, Brian Custodero, John Kanis, Kevin Lo, Mike Tran, Nazilla Rouse, and Miguel Ramsey. The Tyvak team includes Austin Williams, Chris Shaffer, Ricky Prasad, Ehson Mosleh, Jeff Mullen, Jeff Weaver, Sean Fitzsimmons, Nathan Fite, John Brown, John Abel, and Craig Francis.

References

- [1] Hodges, R., Chahat, N., Hoppe, D., and Vacchione, J. "The Mars Cube One Deployable High Gain CubeSat Antenna." *IEEE Antennas and Propagation Magazine*, Forthcoming.
- [2] Mohon, L. NASA's Cubequest Challenge. NASA. http://www.nasa.gov/directorates/spacetech/centennial_challenges/cubequest/index.html. Accessed May 16, 2015.
- [3] Reynolds, W., Murphey, T., and Banik, J. Highly Compact Wrapped-Gore Deployable Reflector.
- [4] Shirvante, V., Johnson, S., Cason, K., Patankar, K., and Fitz-Coy, N. "Configuration of 3U CubeSat Structures for Gain Improvement of S-Band Antennas." *AIAA/USU Conference on Small Satellites*, 2012.

- [5] Babuscia, A., Corbin, B., Knapp, M., Jensen-Clem, R., Van de Loo, M., and Seager, S. "Inflatable Antenna for Cubesats: Motivation for Development and Antenna Design." *Acta Astronautica*, Vol. 91, 2013, pp. 322–332. doi:10.1016/j.actaastro.2013.06.005.
- [6] Aherne, M., Barrett, T., Hoag, L., Teegarden, E., and Ramadas, R. "Aeneas -- Colony I Meets Three-Axis Pointing." *AIAA/USU Conference on Small Satellites*, 2011.
- [7] MacGillivray, C. "Scott." Miniature High Gain Antenna for CubeSats. California Polytechnic State University San Luis Obispo, California, Apr 22, 2011.
- [8] Hodges, R. E., Radway, M. J., Toorian, A., Hoppe, D. J., Shah, B., and Kalman, A. E. ISARA - Integrated Solar Array and Reflectarray CubeSat Deployable Ka-Band Antenna. Presented at the 2015 IEEE International Symposium on Antennas and Propagation USNC/URSI National Radio Science Meeting, 2015.
- [9] Chahat, N., Sauder, J., Mitchell, M., Beidleman, N., and Freebury, G. One-Meter Deployable Mesh Reflector for Deep Space Network Telecommunication at X- and Ka-Band. Presented at the 2019 13th European Conference on Antennas and Propagation (EuCAP), 2019.
- [10] Sauder, J. F., Arya, M., Chahat, N., Thiel, E., Dunphy, S., Shi, M., Agnes, G., and Cwik, T. Deployment Mechanisms for High Packing Efficiency One-Meter Reflectarray Antenna (OMERA). In *AIAA Scitech 2019 Forum*, American Institute of Aeronautics and Astronautics.
- [11] Huang, J., and Encinar, J. A. *Reflectarray Antennas*. Wiley-IEEE Press, Piscataway, N.J. : Hoboken, N.J., 2007.
- [12] Tan, L. T., and Pellegrino, S. Stiffening Method for "Spring-Back" Reflectors. Presented at the IASS-IACM, Athens, Greece, 2000.
- [13] Bassily, S., and Thomson, M. Deployable Reflectors. In *Handbook of Reflector Antennas and Feed Systems Volume 3: Applications of Reflectors*, Artech House, Boston, Massachusetts.
- [14] Davis, G., and Tanimoto, R. Mechanical Development of Antenna Systems. In *Spaceborne Antennas for Planetary Exploration*, John Wiley & Sons.
- [15] UNFURLABLE SPACE REFLECTOR SOLUTIONS. http://download.harris.com/app/public_download.asp?fid=463. Accessed Dec. 5, 2016.
- [16] SMALL SATELLITE ANTENNAS: 1-Meter Unfurlable Mesh Antenna. *Harris Government Communications Systems*. <http://govcomm.harris.com/#1-meter-unfurlable-mesh-antenna>.
- [17] Sauder, J., Chahat, N., Hodges, R., Thomson, M., Rahmat-Samii, Y., and Peral, E. Designing, Building, and Testing a Mesh Ka-Band Parabolic Deployable Antenna (KaPDA) for CubeSats. Presented at the AIAA SciTech, San Diego, 2016.
- [18] Sauder, J., Chahat, N., Hodges, R., Thomson, M., and Rahmat-Samii, Y. Ka-Band Parabolic Deployable Antenna (KaPDA) Enabling High Speed Data Communication for CubeSats. Presented at the SPACE Conferences and Exposition, Pasadena, CA, 2015.
- [19] Chahat, N., Hodges, R. E., Sauder, J., Thomson, M., Peral, E., and Rahmat-Samii, Y. "CubeSat Deployable Ka-Band Mesh Reflector Antenna Development for Earth Science Missions." *IEEE Transactions on Antennas and Propagation*, Vol. 64, No. 6, 2016, pp. 2083–2093. doi:10.1109/TAP.2016.2546306.
- [20] Chahat, N., Sauder, J., Thomson, M., Hodges, R., and Rahmat-Samii, Y. CubeSat Deployable Ka-Band Reflector Antenna for Deep Space Missions. Presented at the 2015 IEEE International Symposium on Antennas and Propagation USNC/URSI National Radio Science Meeting, 2015.
- [21] Milne, J. S., and Kaufman, D. S. *General Environmental Verification Specification*. 2003.
- [22] Peral, E., Tanelli, S., Haddad, Z., Sy, O., Stephens, G., and Im, E. Raincube: A Proposed Constellation of Precipitation Profiling Radars in CubeSat. Presented at the 2015 IEEE International Geoscience and Remote Sensing Symposium (IGARSS), 2015.
- [23] Sauder, J., Chahat, N., Hodges, R., Peral, E., Rahmat-Samii, Y., and Thomson, M. Lessons Learned from a Deployment Mechanism for a Ka-Band Deployable Antenna for CubeSats. In *44th Aerosp. Mech. Symp.*, No. 361, Cleveland, OH, 2018.
- [24] Sauder, J., Chahat, N., Hirsch, B., Hodges, R., Peral, E., Rahmat-Samii, Y., and Thomson, M. From Prototype to Flight: Qualifying a Ka-Band Parabolic Deployable Antenna (KaPDA) for CubeSats. Presented at the 4th AIAA Spacecraft Structures Conference, Orlando, FL, 2017.